Journal of Electroceramics 1:1, 73–89, 1997
© 1997 Kluwer Academic Publishers, Boston. Manufactured in The Netherlands.

The Influence of Laterally Inhomogeneous Contacts on the Impedance of Solid Materials: A Three-Dimensional Finite-Element Study

J. FLEIG & J. MAIER
Max-Planck-Institut für Festkörperforschung, Heisenbergstr. 1, 70569 Stuttgart, Germany
email: fleig@chemix.mpi-stuttgart.mpg.de

Received October 2, 1996; Revised January 13, 1997; Accepted January 13, 1997

Abstract. The total impedance of samples with electrodes exhibiting only partial contact (porous electrodes) is investigated using the finite element method in three dimensions. Emphasis is put on porous electrodes built up of arrays of small perfect contacts. An equivalent circuit to analyze the impedance spectra is put on a firm basis enabling the reliable determination of bulk properties of ''imperfectly'' contacted samples. Approximations are given to estimate the contact geometry impedance. The results are also applicable to other imperfect contact problems as occurring at grain boundaries.

Keywords: impedance, porous electrode, inhomogeneous contact, finite element method, potential distribution, current constriction

1. Introduction

In electroceramics electrode contacts are frequently laterally inhomogeneous, e.g., porous. In some cases these porosities are introduced deliberately as in the case of solid oxide fuel cells. The gas exchange which is essential to operate the cell is ensured by the three phase contacts of the porous electrode geometry. As a consequence, most investigations of gas exchange reactions (e.g., incorporation of oxygen in oxides, incorporation of hydrogen in protonic conductors) concentrate on porous electrodes (see e.g., [1–15]). On the other hand the porosity of electrodes may be an undesired property. Frequently only parts of the electrodes exhibit an intimate contact with the sample while other parts of the sample surface are separated from the electrode by an insulating gap due to insufficient preparation or insufficient wetting properties. A typical example would be a metal foil mechanically pressed onto the sample: a perfect fit of sample and electrode morphology will usually not be achieved. The particles of paste-electrodes may give rise to a similar contact geometry and even evaporated or sputtered electrodes often agglomerate at higher temperatures and form ''islands'' leaving some parts of the surface uncoated (see e.g., [9,10,16]).

A main feature of all these electrodes with laterally inhomogeneous contacts is the frequency-dependence of the current carrying electrode area. An applied dc-voltage leads to a current constriction close to the reversible areas while displacement currents at higher frequencies also include the electrode regions without reversible contact. Thus porous electrodes influence not only the dc-conductivity compared to a homogeneous contact but also the shape of the impedance spectra. The reversible area for dc-current is in some cases given by the contacted electrode regions while frequently complicated reaction mechanisms (e.g., O_2-incorporation in YSZ) are involved leading to a very restricted reversible region close to the three-phase boundary.

There are numerous experiments (e.g., [1–14]) investigating the electrode impedance of porous

electrodes, especially at three-phase-boundaries. Yet, although the electrode impedance of such porous electrodes is characterized by the interplay of constriction resistance and ''real'' electrode polarization only little attention has been paid to the problem in how far the current constriction influences the impedance. In [15] the dc resistance of electrodes with active spots or stripes has been investigated using an electrolytic tank. Thus it could be demonstrated quantitatively how the total resistance depends on the geometry of the porous electrode. Furthermore it could be concluded that a part of the electrode polarization of a Ag, $O_2|YSZ|O_2$, Ag cell is due to current constriction. In [5] the polarization of Au-electrodes on YSZ was examined using an analytical solution for the dc resistance between two electrodes each built up by an array of square contacts. It could be shown that the measured resistance fits nicely to the resistance obtained from these calculations and the entire polarization can be attributed to geometrical effects. The role of active points for the time dependent dissolution of Li at the $Li|Li_3N$ interface and the potential distribution was considered in [17]. An intuitive equivalent circuit model for imperfect (''porous'') electrodes is presented in [17,18].

The problem of porous electrodes is very much related to the situation at grain boundaries in electroceramics. Such grain boundaries could also exhibit both permeable (conducting) regions and insulating parts with respect to current perpendicular to the boundary (island model). They may be constituted e.g., by air gaps (pores), amorphous layers, segregated phases or lattice mismatch. In the case of an alternation of insulating and conducting regions the situation is similar to a porous electrode problem. With respect to grain boundary resistances a large number of publications (e.g., for ZrO_2 and CeO_2 [19–31], AgCl [32]) exist in the literature. Frequently two semicircles in the complex impedance plane are observed, the high frequency semicircle being attributed to the bulk and the second one to grain boundaries. The two resistances often exhibit similar activation energies [22,26–30] and as a reason for this fact imperfect contacts between the grains have been discussed. There are semi-quantitative models [19,20,24,26,27,33–36] to justify this explanation and to enable a correct interpretation of the spectra. However, an exact calculation of the resulting impedance by solving the underlying differential equation and thus providing a founded interpretation of the spectra is still missing.

Further cases exhibiting laterally inhomogeneous contacts are found in the expanding field of composites as e.g., cermets used as anodes in SOFC or heterogeneously doped ionic conductors (e.g., Al_2O_3-AgCl-composites). In the latter case again two semicircles in the complex impedance plane are frequently observed [37].

For all experiments with laterally inhomogeneous contacts a founded estimation of the influence of the contact geometry not only on the dc resistance but on the ac impedance also, would be helpful in order to avoid errors caused by current constriction. Furthermore, the question arises in how far electrical properties can be obtained reliably when ''imperfect'' contacts are present. Two-dimensional calculations on the influence of imperfect contacts on the impedance based solely on Maxwell's equations were given by the authors in [38,39]. As a main result of these finite-element-simulations the occurrence of a second relaxation time (second semicircle in the complex impedance plane) exclusively due to the existence of laterally inhomogeneous contacts could be proved. However, a quantitative investigation of a realistic three-dimensional problem is still missing.

Such a three-dimensional investigation is presented in this contribution. We restrict ourselves to the case of an electrode with laterally inhomogeneous contact and a reversible two-phase-boundary. For the sake of simplicity we neglect all additional electrode polarization processes and emphasize the interplay of morphology and impedance. Two-dimensional calculations on porous electrodes including a polarization impedance are given in [40]. The geometrical and materials parameters will be varied over a wide range to estimate the influence of electrode morphology on the overall impedance and to show how experiments exhibiting current constriction effects should be analyzed.

2. Theoretical and Computational Considerations

Equivalent circuits are useful tools to analyse impedance spectra of materials with regions of different electrical properties as long as the interfaces are parallel to the electrodes (quasi-one-dimensional case). However there is a fundamental problem if

simple equivalent circuits are applied to specimens exhibiting inhomogeneities in electrical properties not only parallel to the electrodes but in arbitrary direction. This problem is connected with inherent assumptions which are made when parallel RC-elements are used to represent sample regions. The following necessary conditions have to be fulfilled if a region is described by a parallel RC-element which

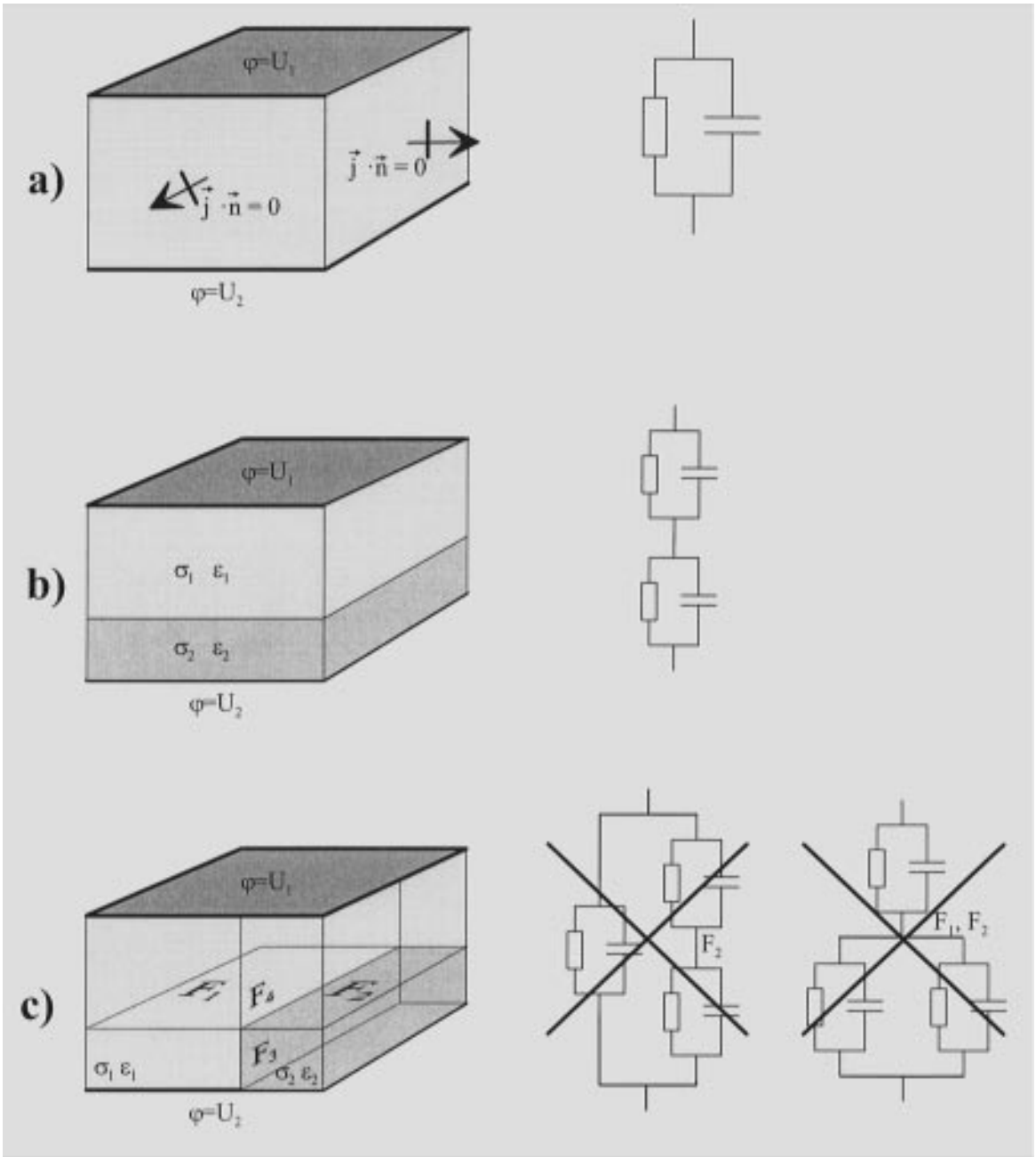

Fig. 1. Sketch to demonstrate the limit of equivalent circuits. (a) The two necessary conditions for a region being replaced by a RC-element. (b) Inhomogeneous sample which can be described by a simple equivalent circuit. (c) Sample for which no simple equivalent circuit is valid.

solely depends on the geometry and the materials parameters of this region (Fig. 1a):

(i) Two opposite surfaces of the region have to be equipotential for all frequencies. (A parallel RC-element is by definition between two points of defined potential.)
(ii) The current density perpendicular to the other surfaces has to vanish.

The replacement is possible e.g., for the quasi-one-dimensional arrangement of two homogeneous phases (Fig. 1b). However, it is not valid for the example shown in Fig. 1c. A simple division of the sample into regions represented by RC-elements is not allowed. Neither are the surfaces F_1 and F_2 equipotential nor are F_3 and F_4 without perpendicular current density. This failure of relating regions of the sample to simple equivalent circuits causes difficulties to predict the impedance of real inhomogeneous samples and to relate the measured impedance to electrical and geometrical properties.

A way out is the calculation of the exact impedance via determining the exact potential distribution within the sample [38]. This implies the numerical solving of the underlying differential equation. As long as time-dependent magnetic fields can be neglected, Poisson's equation can be written in terms of a scalar electrical potential Φ

$$\text{div grad } \Phi(\mathbf{r},t) = -\frac{1}{\varepsilon}\rho(\mathbf{r},t) \tag{1}$$

with ε being the absolute dielectric constant and ρ the charge density. It is well known that the charge density ρ vanishes in the bulk. Space charges close to interfaces we consider as a part of the interface charge and neglect the diffuse character of space charges. Thus Eq. (1) reduces to Laplace's equation

$$\frac{\partial^2\Phi}{\partial x^2}+\frac{\partial^2\Phi}{\partial y^2}+\frac{\partial^2\Phi}{\partial z^2}=0 \tag{2}$$

For an applied ac voltage $U_0 e^{i\omega t}$ of angular frequency ω between the two electrodes the potential Φ within the sample is given in complex representation by

$$\hat{\Phi}(\mathbf{r},t)=\hat{\varphi}(\mathbf{r})e^{i\omega t}\equiv|\hat{\varphi}(\mathbf{r})|e^{i(\omega t+\alpha(\mathbf{r}))} \tag{3}$$

provided the deviations from equilibrium are small (linear regime). (The ''hat'' indicates complex quantities.) In the following there are two reasons for the potential being complex. First its phase changes within the sample as a function of the space-coordinate leading to a position-dependent complex representation, and second the time dependence which is written in a complex way using $e^{i\omega t}$. The phase $\alpha(\mathbf{r})$ of the position-dependent potential $\hat{\varphi}(\mathbf{r})$ should not be confused with the phase shift between total current and applied voltage. The value of $\alpha(\mathbf{r}_2)-\alpha(\mathbf{r}_1)$ describes the phase shift between the potentials at two points $\mathbf{r}_2$ and $\mathbf{r}_1$.

In this contribution all surface (interface) potentials are assumed to be independent of the current, i.e. only the linear regime (small applied voltage) is considered. Consequently without restriction of generality, the surface potentials can be ignored in the calculation of the impedance. Therefore the following boundary conditions are used to calculate the potential by solving Laplace's equation for $\hat{\varphi}(\mathbf{r})$:

(i) Electrode/sample contact: the contacted parts of the solid electrolyte are set on the same potential as the electrodes (0 and $U_0 e^{i\omega t}$ respectively).
(ii) Free sides of the solid electrolyte are without normal current density: grad $\hat{\varphi}\cdot\mathbf{n}=0$, where $\mathbf{n}$ is the normal vector of the relevant side.
(iii) Solid electrolyte/insulator interface: the continuity of the normal component of the complex current density must be warranted:

$$\hat{\kappa}_{bulk}\,\text{grad}\,\hat{\varphi}_{bulk}\cdot n=\hat{\kappa}_{gap}\,\text{grad}\,\hat{\varphi}_{gap}\cdot n \tag{4}$$

The index gap indicates the insulating phase. The complex conductivity $\hat{\kappa}$ is defined by

$$\hat{\kappa}=\sigma+i\omega\varepsilon \tag{5}$$

with σ being the electrical conductivity. Eq. (4) can be derived by combining Poisson's equation (Eq. (1)) and the continuity equation for the Faraday current density (total current density minus displacement current density, i.e., true conducting current density—σ grad $\hat{\Phi}$)

$$\text{div}(\sigma\,\text{grad}\,\hat{\Phi})=\frac{\partial\hat{\rho}}{\partial t} \tag{6}$$

using Eq. (3) and integrating over the surface of a thin volume element at the phase boundary. For the applied voltage $U_0 e^{i\omega t}$ resulting in a total current $\hat{I}_0 e^{i\omega t}$ the complex impedance $\hat{Z}$ between the two electrodes can be calculated as

$$\hat{Z}=\frac{U_0}{\hat{I}_0} \tag{7}$$

with the current $\hat{I}_0$ being given as the surface-integral

$$\hat{I}_0 = \int_s \hat{\mathbf{j}} \cdot d\mathbf{A} \tag{8}$$

of the complex current density

$$\hat{\mathbf{j}} = -\hat{\kappa}\,\mathrm{grad}\,\hat{\varphi} \tag{9}$$

along an arbitrary cross-section of the sample S which does not cross the electrodes. Once the potential distribution $\hat{\varphi}(\mathbf{r})$ is known, the impedance can be calculated for a given complex conductivity as

$$\hat{Z} = \frac{U_0}{\int_s -\hat{\kappa}\,\mathrm{grad}\,\hat{\varphi} \cdot d\mathbf{A}} \tag{10}$$

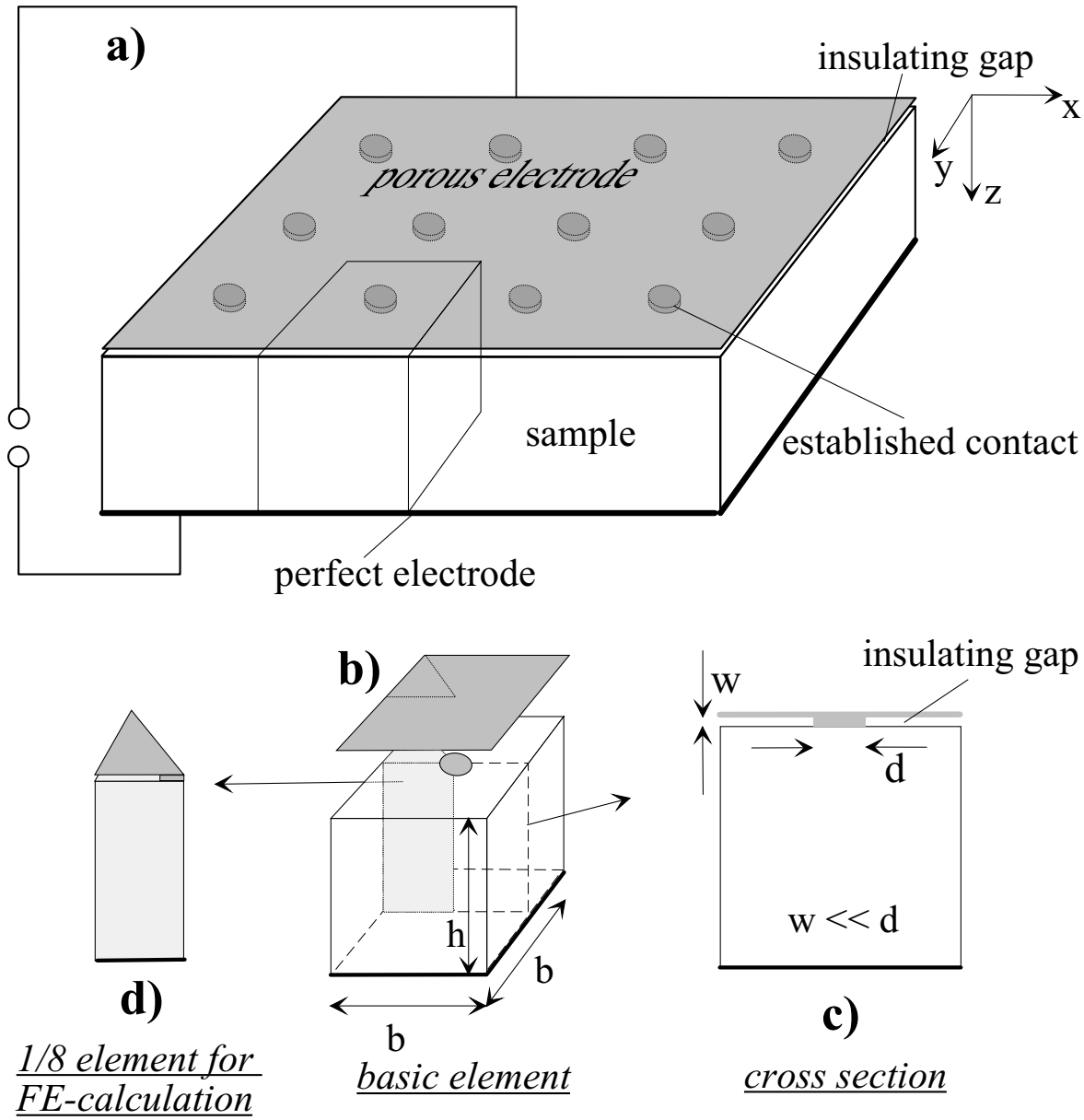

Fig. 2. Geometry of the considered porous electrodes. (a) A sector of the sample with one porous electrode exhibiting only partial contact (circles). (b) A basic element of this set-up. The porous electrode is lifted to illustrate the contacted region. (c) Cross section of the basic element indicating the point diameter *d* and gap thickness *w*. (d) 1/8 of the basic element as used in the finite element calculations.

By varying the frequency and thus the complex conductivity, it is possible to simulate the entire impedance spectrum for a given sample geometry.

We focussed onto a symmetrical prototype of porous electrodes as sketched in Fig. 2: One electrode (bottom electrode in Fig. 2) is assumed to be perfect, i.e., without any electrode polarization, neglecting the resistivity of the electrode material itself. The porous electrode on top exhibits regions at which sample and electrode are separated by an insulating gap (air gap, pore). Since at the contacted regions all additional polarization phenomena (e.g., charge transfer resistance) are neglected, only the interplay of geometry (morphology, porosity) and impedance is considered. In order to reduce the number of geometrical parameters, a constant gap thickness is assumed, giving rise to a step-like arrangement (Fig. 2). Owing to the symmetry of the basic element the three sides of 1/8 of the basic element (Fig. 2d) are without perpendicular current density. Already such an element contains the entire information of the considered system.

For porous electrodes exhibiting very thin air gaps ($w \ll (b-d)$, see Fig. 2c) a further simplification is possible. Instead of treating the air gap as an own phase, it can be taken account of as a boundary condition. As expected on the basis of an intuitive picture and also proven by finite-element calculations, the current within the thin gap flows mainly perpendicular to the boundary as long as the distance between the considered region and the established contact is much larger than the gap thickness. For example, for a gap extended parallel to the *xy*-plane (Fig. 2) the inequality $j_z \gg j_x, j_y$ holds. Thus taking account of Eqs. (2), (3) and (9) the problem reduces to

$$\frac{\partial^2 \hat{\varphi}_{gap}}{\partial z^2} = 0 \tag{11}$$

and the potential distribution within the insulating gap is given as

$$\hat{\varphi}_{gap} \approx \frac{(\hat{\varphi}_{boundary} - U_1)}{w} z + U_1 \tag{12}$$

Therefore the knowledge of the potential at the phase boundary between sample and gap $\hat{\varphi}_{boundary}$ is sufficient to calculate the potential distribution within the gap. Using Eqs. (4), (12) and $U_1 = 0$ a boundary condition for $\hat{\varphi}_{boundary}$ results as

$$\hat{\kappa}_{bulk}\mathbf{n} \cdot \operatorname{grad} \hat{\varphi}_{boundary} = \frac{\hat{\kappa}_{gap}}{w} \hat{\varphi}_{boundary} \tag{13}$$

We compared the potential distributions within samples with porous electrodes calculated via the boundary condition (iii) (Eq. (4)) explicitly taking account of the gap as a separate phase and those calculated by using Eq. (13). As long as $w \ll (b-d)$ is valid, a very slight difference is visible only in the vicinity of the electrode step which is negligible for the overall impedance. Most of the calculations in this contribution were done using the boundary condition Eq. (13) replacing boundary condition (iii) (Eq. (4)).

It is worth mentioning that according to Eqs. (9) and (5) the current density can be written as the sum of four terms

$$\begin{aligned}\hat{\mathbf{j}} = &-\sigma \operatorname{grad} \hat{\varphi}_{re} + \omega\varepsilon \operatorname{grad} \hat{\varphi}_{im} \\ &- i(\sigma \operatorname{grad} \hat{\varphi}_{im} + \omega\varepsilon \operatorname{grad} \hat{\varphi}_{re})\end{aligned} \tag{14}$$

The real part of the current density as well as its imaginary part is a linear combination of the two vectors $\operatorname{grad} \hat{\varphi}_{re}$ and $\operatorname{grad} \hat{\varphi}_{im}$. Thus they are neither perpendicular to the equipotential lines of $\hat{\varphi}_{re}$ nor to those of $\hat{\varphi}_{im}$, and the total current density is no more perpendicular to the equipotential lines of the absolute value of the potential. Looking at the time dependence of the current density vector $\hat{\mathbf{j}}e^{i\omega t}$ one recognizes that it rotates on an ellipse, the main axes of which can be calculated from the real and imaginary part of the current density. The current lines are time-dependent and oscillate between two limiting lines. Consequently, the current density at an arbitrary point generally never vanishes. This is an important difference compared to the one-dimensional case in which for each frequency period the current density vanishes twice. Only if $\operatorname{grad} \hat{\varphi}_{re}$ and $\operatorname{grad} \hat{\varphi}_{im}$ have the same direction (e.g., at the contacted parts of the porous electrode), no change of the current density direction takes place and the current density really vanishes twice a period.

The finite element method was applied to solve the Laplace equation for $\hat{\varphi}(\mathbf{r})$ numerically within the sample. For these simulations the FLUXEXPERT system from DT2i 38240 Meylan, France has been used. The complex current density $\hat{\mathbf{j}}$ and its integral along a surface (e.g., the perfect electrode) could also be obtained by this system. For displaying the resulting potential and current distributions equipotential lines turned out to be more appropriate. In this paper the equipotential lines of the absolute value

of the potential $\sqrt{\hat{\varphi}_{re}^2 + \hat{\varphi}_{im}^2}$ are plotted. The frequency dependent potential distribution and the impedance of samples with one porous electrode (Fig. 2) were calculated for the following range of geometrical (w/b, d/b, h/b) and electrical (σ_{bulk}, σ_{gap}, σ_{bulk}, ε_{gap}) parameters:
$\sigma_{bulk} = 10^{-6}\ (\Omega\text{cm})^{-1}$
$\sigma_{gap} = 0\ (\Omega\text{cm})^{-1}$
$\sigma_{gap} = \varepsilon_0 =$ permittivity of vacuum
$\sigma_{bulk} = (8\text{–}800)\ \varepsilon_0$
$w/b = 1/16\text{–}1/1600$
$h/b = 0.15\text{–}20$
$d/b = 1/20\text{–}1/1.4$
For the complex nonlinear least squares fits of the equivalent circuits to the finite-element results the program ''equivalent circuit'' by B.A. Boukamp [41] has been used.

3. Results and Discussion

Figure 3 illustrates the frequency-dependent potential distribution in 1/8 basic element constituting the sample with a porous electrode as sketched in Fig. 2. The lines in Fig. 3 indicate lines of constant absolute value of the electrical potential and—as the complex potential of the top electrode is set to zero—also the potential drop between the imperfect electrode and the corresponding position within the sample. As already shown in two dimensions [38,39] the main potential

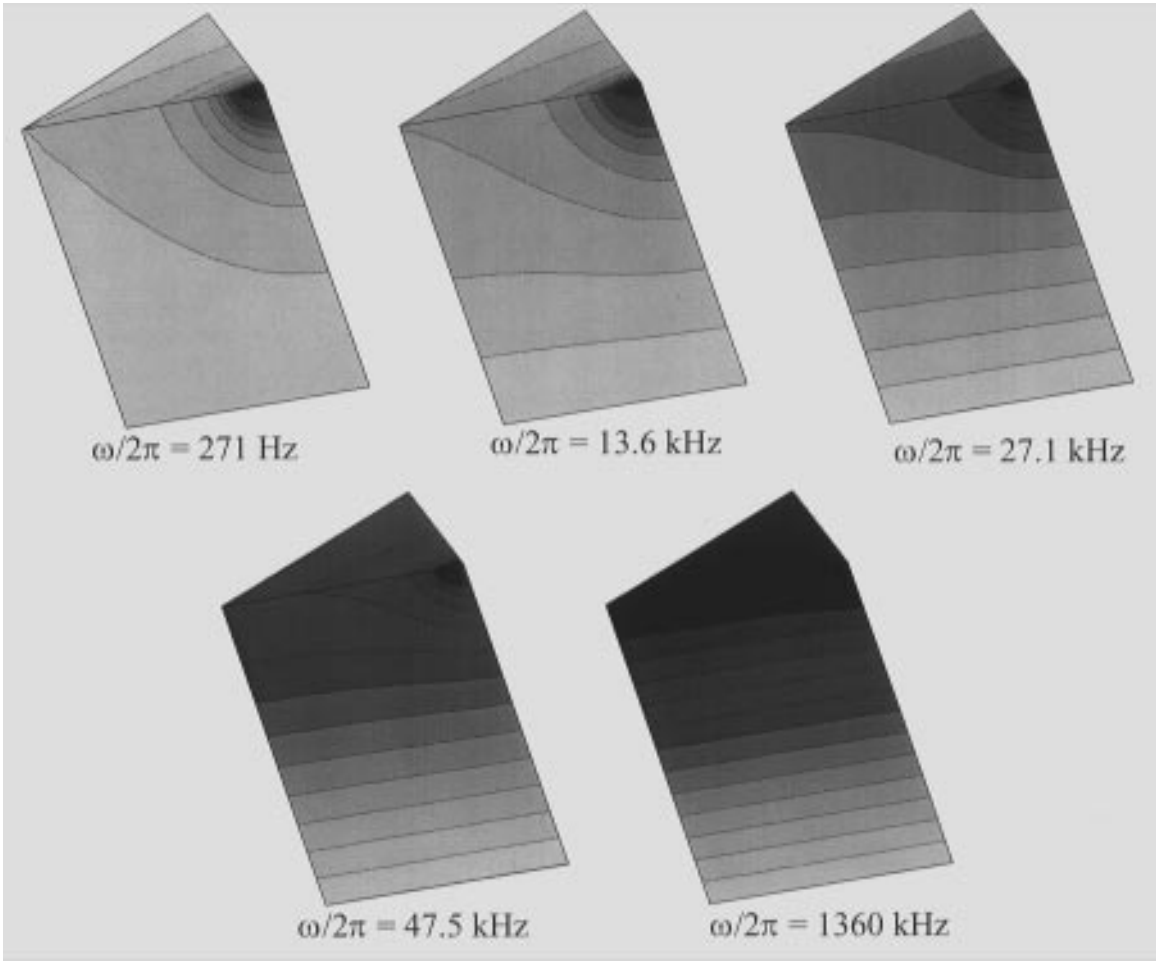

Fig. 3. Equipotential-lines (absolute value of the compex potential) within a 1/8 basic element for five different frequencies. The parameters of the basic element are: $h/b = 0.5$, $d/b = 0.1$, $w/b = 6.3 \times 10^{-4}$, $\varepsilon_{bulk} = 8\varepsilon_0$.

drop at low frequencies occurs in a region around the ''point contact'' whilst at high frequencies the sample behaves nearly as if both electrodes were ideal. This frequency-dependent potential distribution naturally results in an impedance spectrum which is different from the spectrum of a perfectly contacted homogeneous sample (resistance in parallel to a capacitor). Figure 4 shows the impedance obtained by the finite element simulations (FE). Although only one proper relaxation time exists in the material, namely the bulk relaxation time $\tau_{bulk} = \varepsilon_{bulk}/\sigma_{bulk}$, two different relaxation times occur in the spectrum. All the resulting spectra can be fitted nicely (Fig. 5) by the two equivalent circuits given in Fig. 4. Even in the ''worst'' case (the error is larger for thin samples and large points) the fit differs only slightly from the results of the exact finite element calculation (Fig. 5b). It is worth emphasizing that an impedance

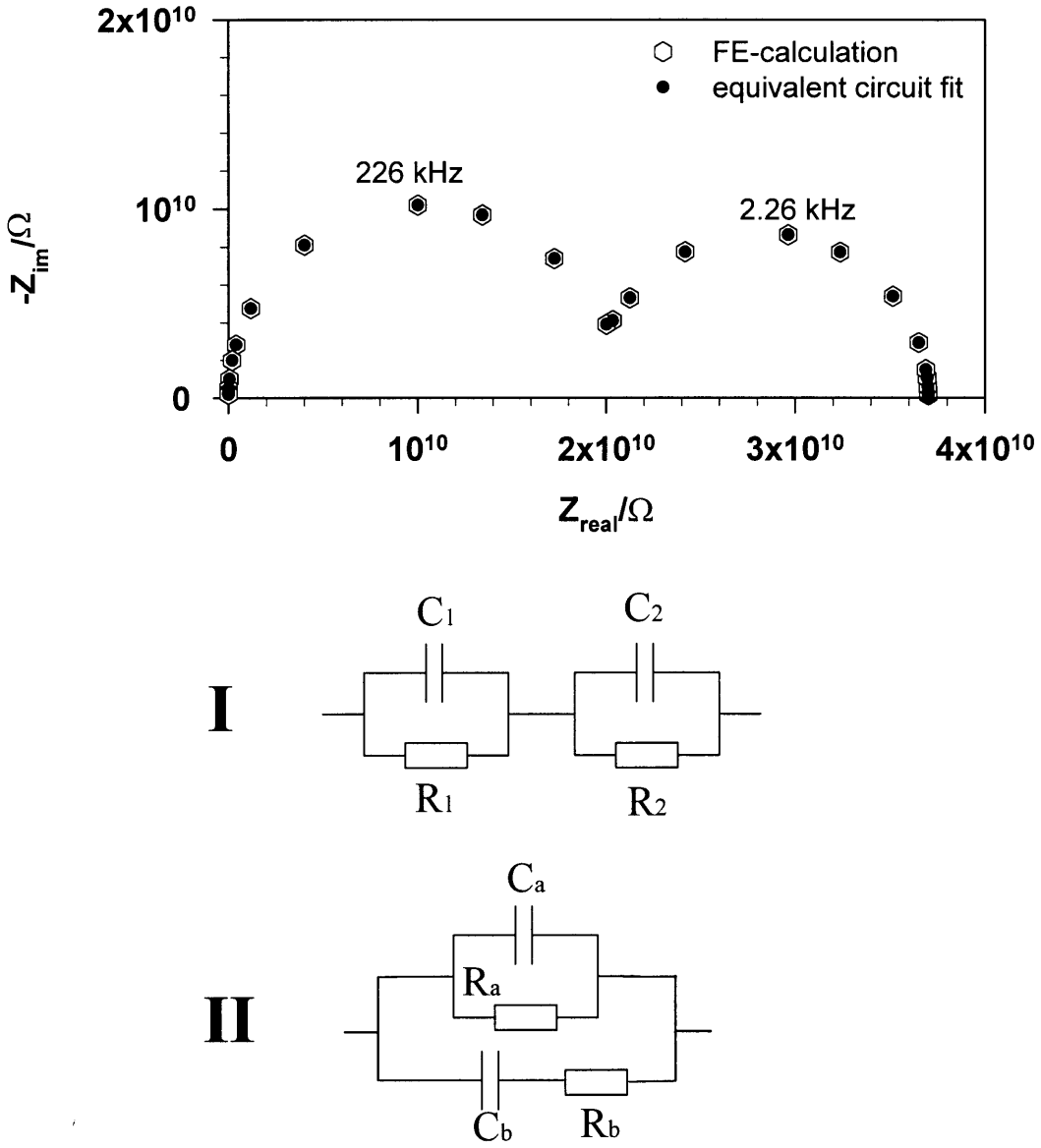

Fig. 4. Impedance spectrum calculated by the finite element method (FE) and the corresponding fit using one of the two possible equivalent circuits I and II. The parameters used are: $h = 100\,\mu$m, $d = 2\,\mu$m, $b = 20\,\mu$m, $w = 0.13\,\mu$m, $\sigma_{bulk} = 10^{-6}$ 1/(Ωcm), $\varepsilon_{bulk} = 8\varepsilon_0$.

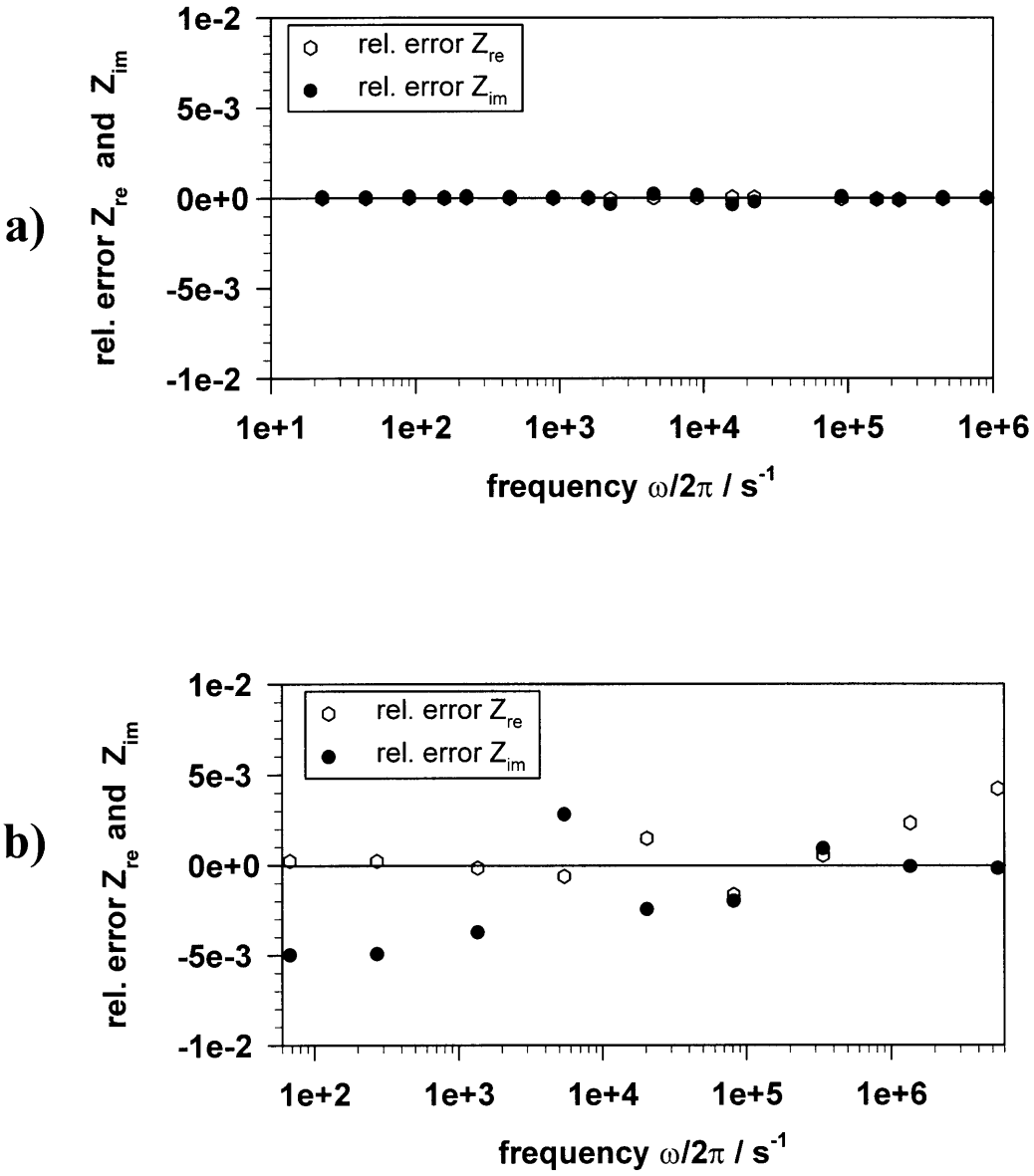

Fig. 5. Relative error of the fit using one of the two equivalent circuits of Fig. 4 compared to the FE-results: $(Z_{re} - Z_{re}^{fit})/Z_{re}$ and $(Z_{im} - Z_{im}^{fit})/Z_{im}$, respectively. (a) Average sample (parameters as in Fig. 3). (b) Calculated impedance with the largest fit error obtained in this work. Parameters: $h/b = 0.15$, $d/b = 0.7$, $w/b = 6.3 \times 10^{-4}$, $\varepsilon_{bulk} = 8\varepsilon_0$.

according to two RC-elements is more or less surprising. The interpretation of these elements is not trivial as will be shown.

In the following, all resistances and capacitances correspond to 1/8 of a basic element, i.e., the region for which the potential distribution is calculated. The impedance Z^{sample} of a sample consisting of N basic elements (N contacts) is just $1/(8N)$ times the impedance calculated by using the region shown in Fig. 3. Therefore all sample resistances R_i^{sample} and capacitances C_i^{sample} are given by $C_i^{sample} = 8NC_i$ and $R_i^{sample} = R_i/8N$.

First the question arises which equivalent circuit given in Fig. 4 should be preferred to analyse the data since both yield identical fit errors and can be transferred into each other [42]. As an example.

Table 1.

R_a	$37.02 \times 10^9\Omega$	R_1	$20.00 \times 10^9\Omega$	R_{bulk}	$20.00 \times 10^9\Omega$
R_b	$64.15 \times 10^9\Omega$	R_2	$17.02 \times 10^9\Omega$	R_{pe}	$20.00 \times 10^9\Omega$
C_a	32.4×10^{-18}F	C_1	35.2×10^{-18}F	C_{bulk}	35.2×10^{-18}F
C_b	62.2×10^{-18}F	C_2	399×10^{-18}F	C_{gap}	350×10^{-18}F
$R_a\|\|R_b$	$23.47 \times 10^9\Omega$				

Fit parameters according to the equivalent circuits of Fig. 4 for the impedance spectrum of 1/8 of a basic element of a sample (Fig. 2d), calculated by the finite element method, with the following geometrical and materials parameters: $h = 100\,\mu$m, $b = 20\,\mu$m, $d = 2\,\mu$m, $w = 1.26\,\mu$m, $\sigma_{bulk} = 10^{-6}$ 1/(Ωcm), $\varepsilon_{bulk} = 8\varepsilon_0$. $R_a||R_b$ means parallel connection of R_a and R_b. The symbols R_{bulk}, C_{bulk}, R_{pc} and C_{gap} are defined in the text.

Table 1 shows the fit values for a spectrum and some R, C-values which would have simple meanings: R_{bulk}, C_{bulk} are the bulk values of 1/8 of a basic element

$$R_{bulk} = 8\frac{1}{\sigma_{bulk}}\frac{h}{b^2} \tag{15}$$

$$C_{bulk} = \frac{1}{8}\varepsilon_{bulk}\frac{b^2}{h} \tag{16}$$

while R_{pc} is 8 times the resistance between a circular electrode with diameter d on top of a semi-infinite sample and an infinitely remote counter-electrode (often called spreading resistance) [43] given by

$$R_{pc} = 8\frac{1}{\sigma_{bulk}}\frac{1}{2d} \tag{17}$$

C_{gap} is the capacitance one would obtain for a plate capacitor with the air gap as dielectric calculated as

$$C_{gap} = \frac{1}{8}\varepsilon_{gap}\frac{b^2 - \pi d^2/4}{w} \tag{18}$$

Table 1 clearly indicates that only for the serial connection of two RC-elements at least two of the elements have a simple meaning: R_1 and C_1 turn out to be always identical to the values of a perfectly contacted sample (R_{bulk} and C_{bulk}). Thus in the following all spectra are analysed via the equivalent circuit I in Fig. 4.

The values of R_1 and C_1 can be attributed to a perfectly contacted bulk and show no dependence on the contact geometry while R_2 and C_2 are determined by the contact geometry (and the materials parameters). In the following we demonstrate how R_2 and C_2 depend on the various parameters and how a rough estimation of these values is achieved.

(a) The Contact Geometry Resistance R_2

First, the relation of R_2 and the bulk conductivity σ_{bulk} will be discussed. The dc-value of the impedance $R_{\omega=0}$ is the sum of R_1 and R_2. Due to the identity of R_{bulk} and R_1 the resistance R_2 (in the following called ''contact geometry resistance'') is just given by

$$R_2 = R_{\omega=0} - R_{bulk} \tag{19}$$

$R_{\omega=0}$ can be calculated without boundary condition iii) (see section 2). Consequently neither the differential equation Eq. (2) nor the boundary conditions include the materials parameters σ and ε, and the dc potential distribution $\phi(x, y, z)$ is solely a function of the geometry. Hence, Eq. (10) can be written as

$$R_{\omega=0} = \frac{1}{\sigma_{bulk}} \cdot f_{geo} \tag{20}$$

where f_{geo} is a purely geometrical factor, viz

$$f_{geo} = \frac{1}{-\int_s \operatorname{grad}\frac{\varphi}{U_0} \cdot d\mathbf{A}} \tag{21}$$

Therefore, the resistance R_2 is also proportional to $1/\sigma_{bulk}$ and using Eq. (19) R_2 can be calculated as

$$R_2 = \frac{1}{\sigma_{bulk}}\left(f_{geo} - \frac{8h}{b^2}\right) \tag{22}$$

This means, that R_2 always exhibits the same conductivity dependence as R_1 and—for a temperature-independent geometry—also the same temperature dependence as experimentally found in many examples for grain boundary contacts [22,26–30] or electrode contacts [5,18,39]. That has also been deduced from intuitive models, however here the precise correlation has been made clearer.

To discuss R_2 as a function of the geometrical parameters we use the length b of a basic element to

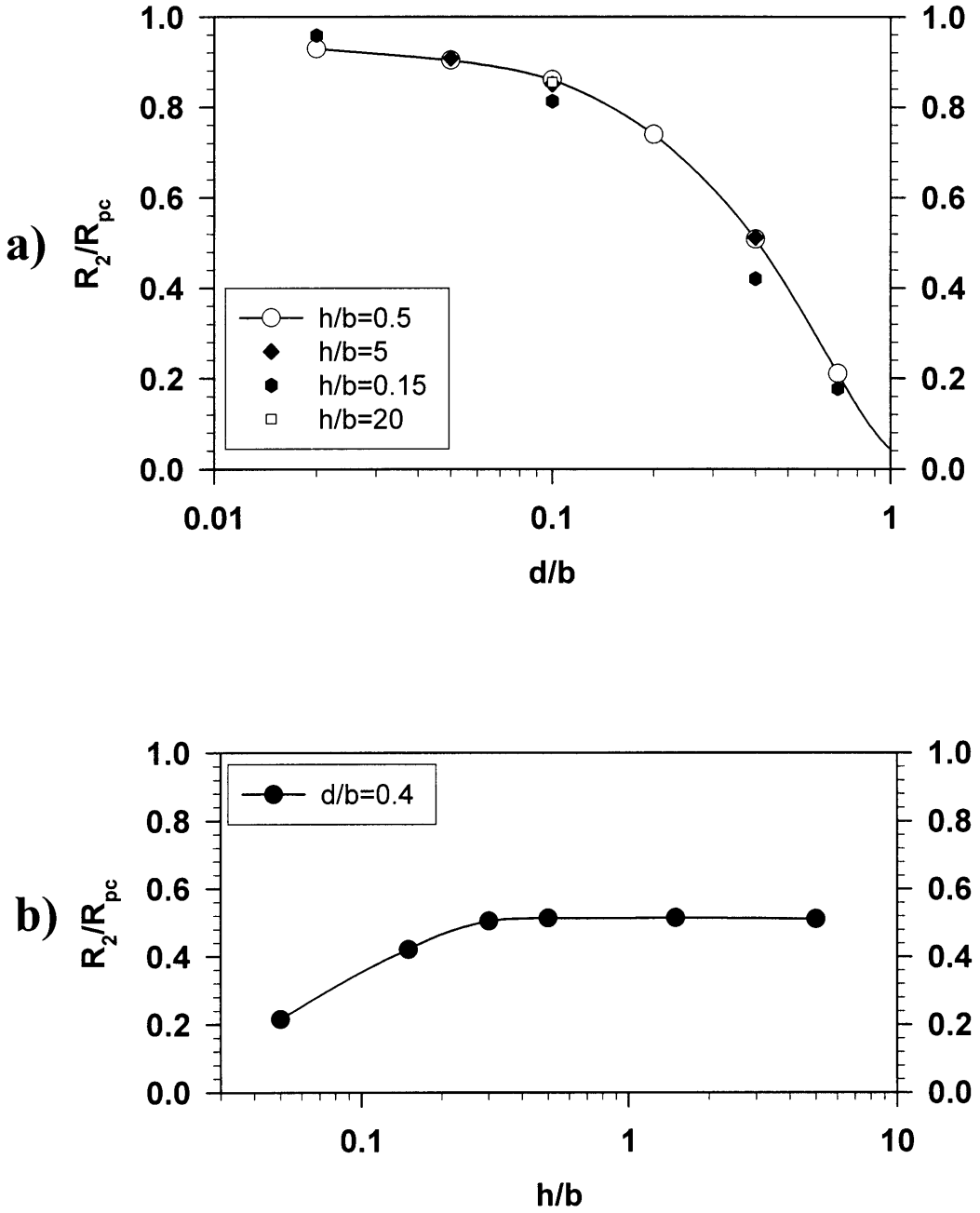

Fig. 6. Contact geometry resistance R_2 normalized with respect to R_{pc} as a function of the relative point diameter d/b (a) and the relative sample height h/b (b). The figure illustrates the limits of the approximation $R_2 \approx R_{pc}$.

normalize the other geometrical quantities w, h and d. As can be seen in Table 1 the resistance R_2 is at least similar to the point contact resistance R_{pc}. In Fig. 6 it is demonstrated in how far R_{pc} can be used as an approximation for R_2 considering the ratio R_2/R_{pc} as a function of geometry. (The normalized point diameter d/b and the normalized sample thickness h/b are the relevant parameters for R_2.) As illustrated in Fig. 6a, R_2/R_{pc} is close to unity for small point contacts ($d/b \ll 1$) but decreases with increasing d/b. This is

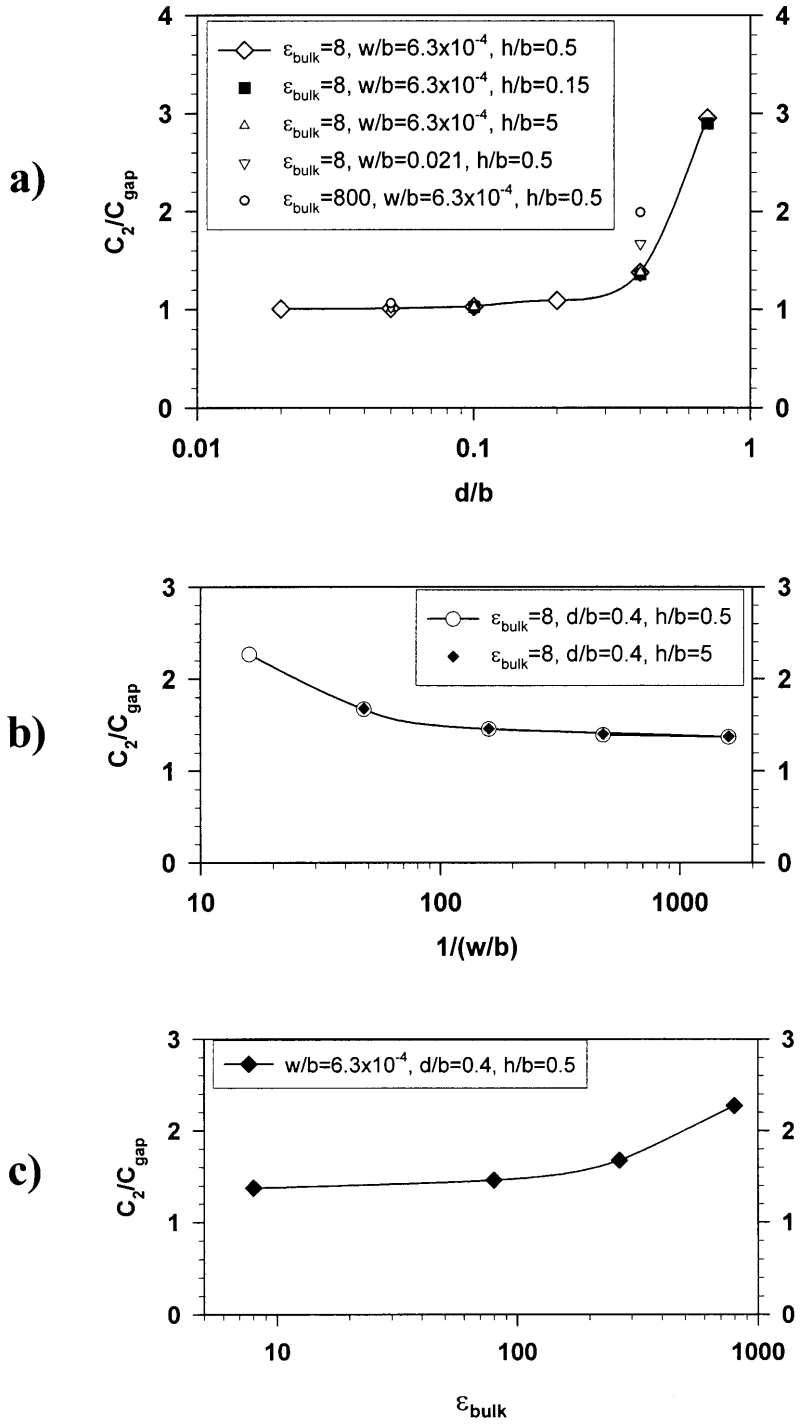

Fig. 7. Capacitance C_2 normalized with respect to the gap capacitance C_{gap} as a function of the relative point diameter d/b (a), the relative gap thickness w/b (b) and the bulk permittivity ε_{bulk} (c). The figure illustrates the similarities but also the differences between C_2 and C_{gap}.

valid for all sample thicknesses (h) considered. On the other hand R_2/R_{pc} is almost independent of the normalized sample thickness as long as the samples are not too thin (compared to the point distance). Thus for a rough estimate of the influence of the current constriction due to the contact ''points'', the relation

$$R_2 \approx R_{pc} \tag{23}$$

can be used as long as the sample is not very thin and the ''points'' are not too large compared to the distance of the contact points. Using Eq. (23) and $R_1 = R_{bulk}$, the approximation

$$\frac{R_2}{R_1} \approx \frac{1}{2}\frac{b}{d}\frac{b}{h} \tag{24}$$

allows us to assess how far the contact geometry resistance R_2 plays a role with respect to the bulk resistance. A more accurate estimate of the factor f_{geo} is given in [44,45].

(b) The Capacitance C_2

As already seen from Table 1 C_2 is close to C_{gap}. This turns out to be the case for the entire parameter range considered in this contribution (see Fig. 7). However, C_2 is not identical to the gap capacitance and shows a non-trivial dependence on the other parameters. For small ''points'' ($d/b \ll 1$) C_2 depends only slightly on d/b, for larger ''points'' it surprisingly increases while the corresponding gap capacitance decreases. Consequently the ratio C_2/C_{gap} increases with increasing point diameter (Fig. 7a). Although the dependence on the gap thickness w shows again a close relationship to C_{gap} (Fig. 7b) the varying ratio C_2/C_{gap} for increasing gap thickness w contradicts an identification of C_2 with C_{gap}. Beyond that C_2 depends slightly on the bulk permittivity (Fig. 7c) emphasizing that a simple interpretation of C_2 is not possible. However, similar to R_2 the capacitance C_2 can be approximated by

$$C_2 \approx C_{gap} \tag{25}$$

as long as d/b is not close to unity.

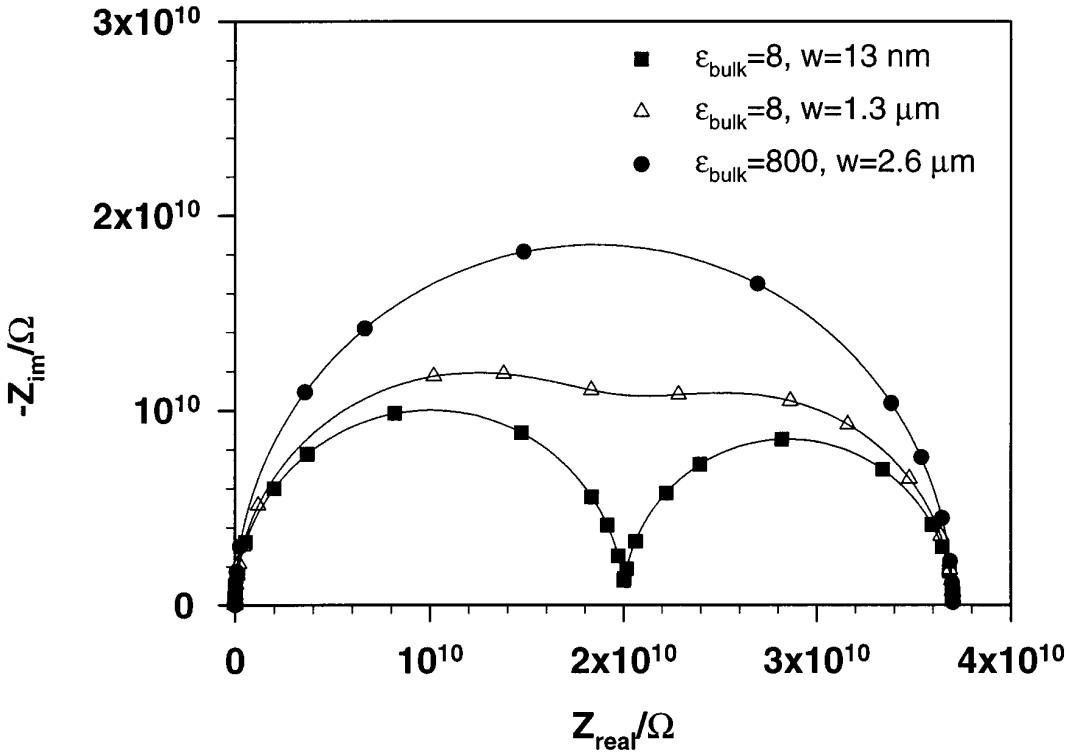

Fig. 8. Impedance spectra for three samples of different gap thickness w and bulk permittivity. All other parameters are the same for the three spectra: $\sigma_{bulk} = 10^{-6}$ 1/(Ωcm), $h = 100\,\mu$m, $b = 20\,\mu$m, $d = \mu$m. The shape of the spectra switches from two to one semicircles.

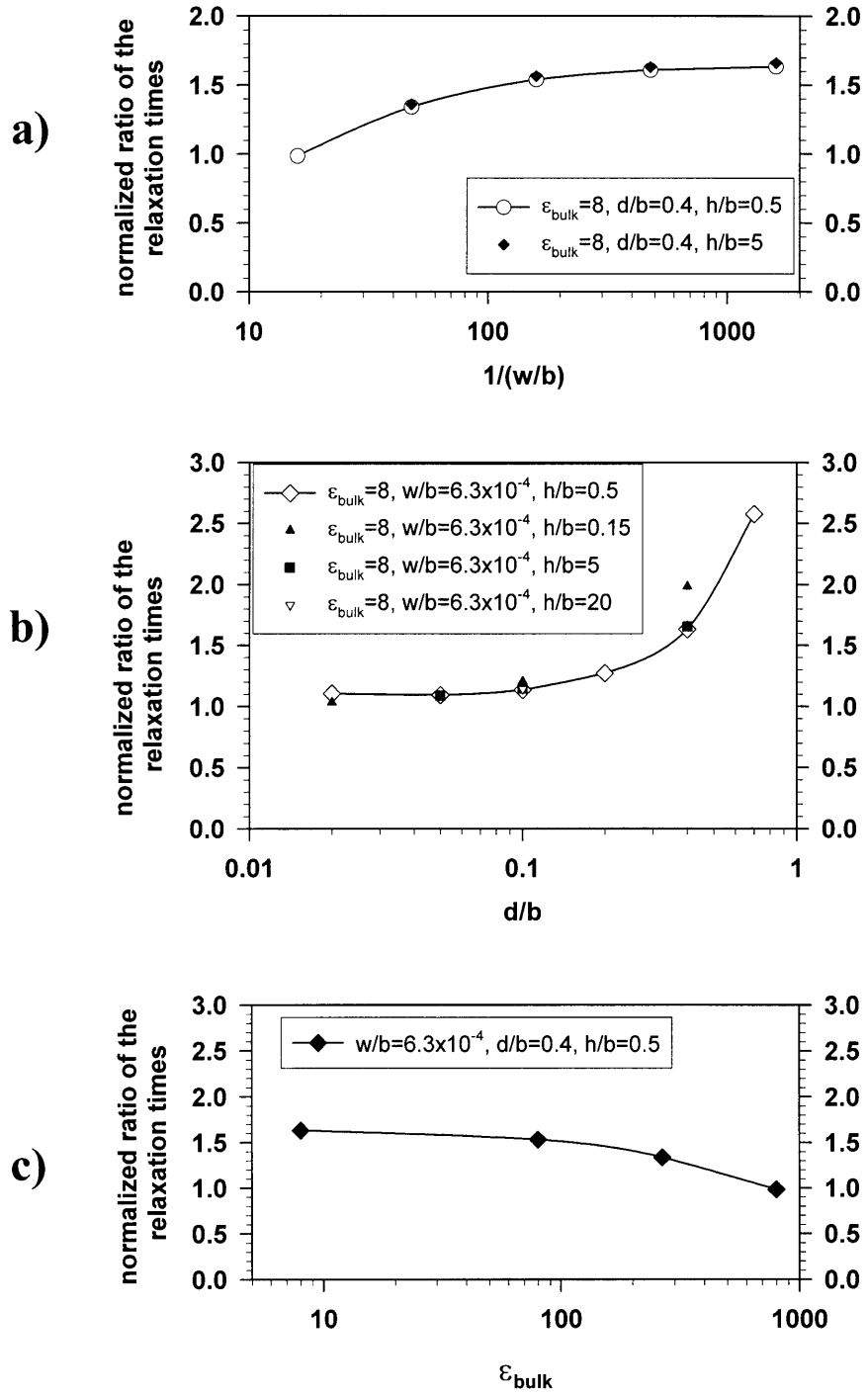

Fig. 9. Ratio of the relaxation times for different relative gap thickness w/b (a), relative point diameter d/b (b) and bulk permittivities ε_{bulk}. The ratio τ_1/τ_2 is normalized with respect to the approximation $2\varepsilon_{bulk}/\varepsilon_{gap}wd/b^2$ (Eq. (26)).

(c) The Relaxation Time τ_2

A further question is whether or not the influence of the contact geometry resistance is always visible as a second semicircle in the complex impedance plane. Figure 8 exemplarily shows that varying the gap thickness w and the bulk permittivity ε_{bulk} can lead to a change from two to one semicircle. (Of course the dc resistance remains unchanged.) Therefore as the last interesting parameter for estimating the consequence of a porous electrode on the impedance, the ratio of the relaxation times $\tau_i = R_i/C_i$ is considered. It indicates whether or not the contact geometry resistance is reflected by a second semicircle. Using the approximations according to Eqs. (23) and (25) the ratio τ_1/τ_2 can be estimated as

$$\frac{\tau_1}{\tau_2} \approx \frac{\varepsilon_{bulk}}{\varepsilon_{gap}} 2 \frac{w}{b} \frac{d}{b} \tag{26}$$

As shown in Fig. 9 the values given by Eq. (26) differ—relatively speaking—from the exact values τ_1/τ_2 even less than R_2 from R_{pc} and C_2 from C_{gap} do (deviations partially cancel). Thus for the entire parameter range considered in this contribution (besides d/b close to 1) Eq. (26) yields a satisfying estimate of the relation time of the second semicircle.

According to Eq. (26) particularly large bulk permittivities could lead to a single semicircle in the complex impedance plane, the meaning of which could be easily misunderstood by that a considerable change of the total resistance due to current constriction is present. In such cases the obtained capacitance is no longer the bulk capacitance and can be even lower than C_{bulk}.

4. Impact on Further Laterally Inhomogeneous Contacts

In section 3 a laterally constant gap thickness w was assumed and the calculations showed that the capacitance C_2 and the relaxation time τ_2 strongly depend on w. Consequently a laterally variable gap thickness will influence the shape of the spectra. As calculated for two dimensions [38] an electrode bent between two contact regions leads to a depression of the contact geometry semicircle and thus to a frequency dependent capacitance.

As already mentioned in the Introduction, three-phase boundary experiments in solid state ionics are also characterized by laterally inhomogeneous contacts. However, here a more complicated situation is met: it is not the entire contacted area which is reversible for dc current but only a narrow ring close to its edge. As a first approximation the rest of the contacted area can be regarded as a very thin insulating layer (blocking electrode). Consequently a further boundary condition of the kind of Eq. (13) has to be introduced for this part. Thus for dc potential the current constriction is even more pronounced while for higher frequencies the very thin insulating layer at the contacted area is short-circuited via displacement current and a situation similar to the one considered in this paper is to be expected. For high frequencies the entire electrode should be current-carrying and a high-frequency semicircle with values identical to the bulk values should be observed. The situation is even more complicated by the presence of an additional polarization (e.g., charge transfer) at the three-phase-

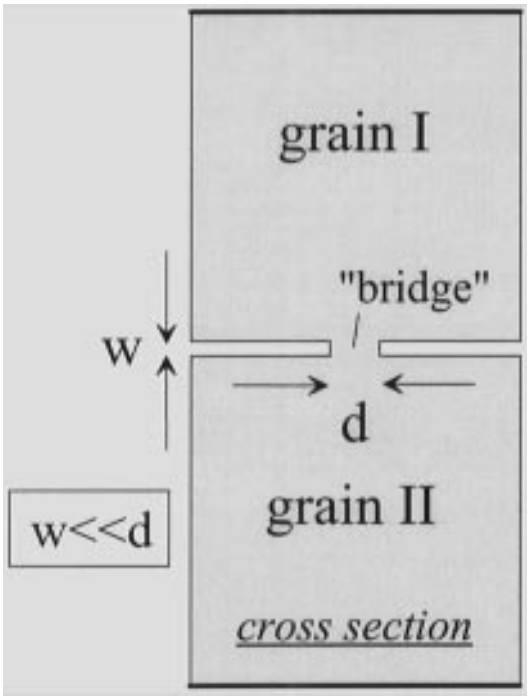

Fig. 10. Cross section of the basic element for a single ''grain boundary'' with insulating gaps corresponding to the similar element for a porous electrode in Fig. 2c. The problem is symmetrical and can be reduced to the element in Fig. 2c as long as $w \ll d$ is valid.

boundary. In [40] an example of a laterally inhomogeneous contact with additional electrode polarization is discussed in two dimensions.

As shown in Fig. 10 the results given in this paper are also valid for grain boundary contacts with insulating inclusions. In order to ''produce'' a partially contacted grain boundary, the electrode material is replaced by material of the same phase. As long as the gap thickness is much smaller than the point diameter the impedance of this ''bridge'' can be neglected and the resulting overall impedance is just twice the impedance of the related porous electrode. This highlights again the fact that R_2 is not a consequence of the ''bridge'' between the two crystals but occurs even for negligible ''bridge'' thickness w.

5. Conclusions

By three-dimensional finite element calculations it could be shown that porous electrodes on electroceramics can lead to two relaxation times in the impedance spectra (two semicircles in the complex impedance plane). Compared to two-dimensional calculations [38,39] the constriction effects are even more pronounced in three dimensions while qualitative differences are not observed. A serial connection of two RC-elements enables a simple interpretation or estimation of the elements for a steplike electrode.

- The high-frequency resistance and capacitance are identical to the values of a perfectly contacted sample (as long as a fit using two serial RC-elements is possible).
- The low-frequency resistance R_2^{sample} is proportional to the bulk resistivity. In turn, a similar temperature dependence of the resistances of both semicircles in the complex impedance plane indicates the existence of geometrically imperfect contacts. However, identical activation energies are not sufficient for such an interpretation: A depletion layer at the interface may yield the same result in some cases [32].
- The low-frequency resistance can roughly be approximated by $R_2^{sample} \approx 1/(2Nd\sigma_{bulk})$ ($N =$ number of contacts, $d =$ point diameter).
- The low-frequency capacitance C_2^{sample} depends on the geometrical parameters as well as on the bulk and gap permittivity. However, it can be roughly approximated by the gap capacitance $C_2^{sample} \approx \varepsilon_{gap}A/w$ ($A =$ gap area, $w =$ gap thickness).

Thus, the magnitude of the contact geometry resistance as well as the corresponding relaxation time can be predicted and a tool to estimate the influence of porous electrodes onto the overall impedance is given.

Acknowledgment

The authors gratefully acknowledge many fruitful discussions with Janez Jamnik, MPI für Festkörperforschung, Stuttgart.

References

1. B.A. Boukamp, B.A. van Hassel, I.C. Vinke, K.J. de Vries, and A.J. Burggraaf, *Electrochimica Acta*, **38**, 1817 (1993).
2. J.G. Fletcher, A.R. West, and J.T.S. Irvine, *J. Electrochem. Soc.*, **142**, 2650 (1995).
3. H.Y. Lee, W.S. Cho, S.M. Oh, H.-D. Wiemhöfer, and W. Göpel, *J. Electrochem. Soc.*, **142**, 2659 (1995).
4. J. Mizusaki, H. Tagawa, K. Tsuneyoshi, and A. Sawata, *J. Electrochem. Soc.*, **138**, 1867 (1991).
5. T. Kenjo and T. Nakagawa, *J. Electrochem. Soc.*, **143**, L92 (1996).
6. D.Y. Wang, *J. Electrochem. Soc.*, **126**, 1166 (1979).
7. J. Mizusaki, K. Amano, S. Yamauchi, and K. Fueki, *Solid State Ionics*, **22** 323 (1987).
8. T. Kenjo, Y. Horiuchi, and S. Osawa, *J. Electrochem. Soc.*, **137**, 2423 (1990).
9. A.J.A. Winnubst, A.H.A. Scharenborg, and A.J. Burggraaf, *Solid State Ionics*, **14**, 319 (1984).
10. W.C. Maskell, N.M. Sammes, and B.C.H. Steele, *J. Phys. D: Appl. Phys.*, **20**, 99 (1987).
11. E.J.L. Schouler and M. Kleitz, *J. Electrochem. Soc.*, **134**, 1045 (1987).
12. S.P.S. Badwal, H.J. de Bruin, and A.D. Franklin, *Solid State Ionics*, **9/10**, 973 (1983).
13. M.J. Verkerk and A.J. Burggraaf, *J. Electrochem. Soc.*, **130**, 78 (1983).
14. D. Braunshtein, D.S. Tannhauser, and I. Riess, *J. Electrochem. Soc.*, **128**, 82 (1981).
15. H. Tannenberger and H. Siegert, *Advances in Chemistry*, **90**, 281 (1969).
16. K.T. Miller, F.F. Lange, and D.B. Marshall, *J. Mater. Res.*, **5**, 151 (1990).
17. M. Meyer, H. Rickert, and U. Schwaitzer, *Solid State Ionics*, **9/10**, 689 (1983).
18. U. Lauer and J. Maier, *J. Electrochem. Soc.*, **139**, 1472 (1992).
19. M. Kleitz, H. Bernard, E. Fernandez, and E. Schouler, in *Advances in Ceramics, Vol. 3, Science and Technology of*

Zirconia, A.H. Heuer and L.W. Hobbs), p.310 (The Am. Ceram. Soc., Washington, DC., 1981).
20. M. Kleitz, C. Pescher, and L. Dessemond, p. 593 in *Science and Technology of Zirconia V*, S.P.S. Badwal, M.J. Bannister and R.H.J. Hannik, eds., (Technomic Publishing Company, Lancaster, PA, USA, 1993).
21. S.P.S. Badwal, J. Drennan, R.H.J. Hannink, and A.E. Hughes, *Key Engineering Materials*, **111/112**, 109 (1995).
22. E.J.L. Schouler, N. Mesbahi, and G. Vitter, *Solid State Ionics*, **9/10**, 989 (1983).
23. K. Yamashita, K.V. Ramanujachary, and M. Greenblatt, *Solid State Ionics*, **81**, 53 (1995).
24. J.E. Bauerle, *J. Phys. Chem. Solids*, **30**, 2657 (1969).
25. S.P.S. Badwal, *Appl. Phys.*, **A50**, 449 (1990).
26. S.P.S. Badwal, *Solid State Ionics*, **76**, 67 (1995).
27. M.J. Verkerk, B.J. Middelhuis, and A.J. Burggraaf, *Solid State Ionics*, **6**, 159 (1982).
28. K. El Adham and A. Hammou, *Solid State Ionics*, **9/10**, 905 (1983).
29. S.P.S. Badwal and J. Drennan, *J. Mat. Sci.*, **22**, 3231 (1987).
30. V.D. Patton, C.C. Wang, S.A. Akbar, and M.A. Alim, *J. Appl. Phys.*, **78**, 1757 (1995).
31. R. Gerhardt and A.S. Nowick, *J. Am. Ceram. Soc.*, **69**, 641 (1986).
32. J. Maier, *Ber. Bunsenges. Phys. Chem.*, **90**, 26 (1986).
33. E.M. Skou and T. Jacobsen, *Appl. Phys.*, **A49**, 117 (1989).
34. P.G. Bruce and A.R. West, *J. Electrochem. Soc.*, **130**, 662 (1983).
35. M. Kleitz, L. Dessemond, and M.C. Steil, *Solid State Ionics*, **75**, 107 (1995).
36. L. Dessemond, R. Muccillo, M. Henault, and M. Kleitz, *Appl. Phys.*, **A57**, 57 (1993).
37. J. Maier, *Prog. Solid St. Chem.*, **23**, 171 (1995).
38. J. Fleig and J. Maier, *Electrochim. Acta*, **41**, 1003 (1996).
39. J. Fleig and J. Maier, *Solid State Ionics*, **85**, 17 (1996).
40. J. Fleig and J. Maier, *Solid State Ionics* (in press).
41. B.A. Boukamp, *Solid State Ionics*, **20**, 31 (1986).
42. J.R. Macdonald and D.R. Franceschetti p. 98 in *Impedance Spectroscopy*, J.R. Macdonald ed. (John Wiley & Sons, New York, 1987).
43. J.W. Orton and P. Blood p. 54 in *The Electrical Characterisation of Semiconductors* (Academic Press, London, 1990).
44. J. Fleig and J. Maier, submitted to Proc. of the Fifth International Symposium on Solid Oxide Fuel Cells (1997).
45. J. Fleig and J. Maier, in preparation.